RESEARCH PAPER

Fabrication, Microstructural Characterization, and Ablation Behavior of a Novel 3D Orthogonal Woven C/C-SiC-ZrB_2 Composite through I-CVI, SI, and LSI Combined Processes

Amin Rezaei[1], Malek Naderi[2,*], Reza Aliasgarian[3], Yousef Safaei[4]

* *mnaderi@aut.ac.ir*

[1] PhD Candidate, Department of Materials and Metallurgical Engineering, Amirkabir University of Technology, Tehran, Iran
[2] Full Professor, Department of Materials and Metallurgical Engineering, Amirkabir University of Technology, Tehran, Iran
[3] PhD, Department of Materials and Metallurgical Engineering, Amirkabir University of Technology, Tehran, Iran
[4] PhD Candidate, Isfahan University of Technology, Faculty of Material Engineering, Isfahan Province, IR 8415683111

Received: January 2025 **Revised: May 2025** **Accepted: June 2025**
DOI: 10.22068/ijmse.3880

Abstract: *This paper presents the novel fabrication method of a three-dimensional orthogonally woven (3DW) C/C-SiC-ZrB_2 composite and the effects of ZrB_2 and SiC particles on microstructure and the ablation behavior of the C/C–SiC–ZrB_2 composite are studied. C/C–SiC–ZrB_2 composite was prepared using an isothermal-chemical vapor infiltration (I-CVI), slurry infiltration (SI), and liquid silicon infiltration (LSI) combined process. Pyrolytic carbon (PyC) was first infused into the 3DW preform by I-CVI at 1050°C using CH_4 as a precursor to form a C/C preform with porous media. The next step was graphitization at 2400°C for 1hr. Then ZrB_2 was introduced into 3DW C/C preform with a void percentage of 48 by impregnating the mixture of ZrB_2 and phenolic resin, followed by a pyrolysis step at 1050°C. A liquid Si alloy was infiltrated, at 1650°C, into the 3DW C/C composites porous media containing the ZrB_2 particles to form a SiC–ZrB_2 matrix. An oxyacetylene torch flame was utilized to investigate the ablation behavior. ZrB_2 particles and the SiC matrix between carbon fiber bundles form a compact ZrO_2-SiO_2 layer. This layer acts as a barrier, restricting oxygen infiltration into the composite and reducing the erosion of carbon fibers. The findings were supported by FESEM imaging and further confirmed through X-ray diffraction and EDS analysis. The addition of ZrB_2 to the C/C-SiC composite resulted in a lower mass and linear ablation rate, 2.20 mg/s and 1.4 µm/s, respectively, while those for the C/C-SiC composite were 4.8 mg/s and 6.75 µm/s after ablation under an oxyacetylene flame (2500°C) for 120 s.*

Keywords: *Three-dimensional orthogonal woven preform, Liquid silicon infiltration, Ceramic-matrix composite, C/C–SiC–ZrB_2 composite, Ablation resistance.*

1. INTRODUCTION

Continuous carbon fiber-reinforced (CFC) SiC–ZrB_2 matrix composites have attracted considerable attention for Ultrahigh-temperature applications due to their superior characteristics, such as low density, low thermal expansion coefficient, high-temperature mechanical strength, excellent thermal shock resistance, high thermal conductivity, and high modulus [1–3]. CFC preform structures, encompassing two-dimensional (2D) laminated forms and three-dimensional (3D) composites, can be produced using techniques like stitching, weaving, braiding, knitting, and needle punching. [4–6]. The three-dimensional orthogonal woven (3DW) preform has a simple fabrication method and relatively good mechanical properties, but a high production cost.

Several techniques have been explored to incorporate SiC-ZrB_2 ceramics into CFC composites, including chemical vapor infiltration (CVI) [7], polymer infiltration and pyrolysis (PIP) [8], liquid silicon infiltration (LSI) [9], and slurry infiltration (SI) [10]. Among these, the LSI method is known for being fast, straightforward, and cost-effective while achieving high densification, which has drawn significant attention from researchers [11–13]. Wang et al. [11] produced a Cf/C-SiC-ZrC composite using a combination of CVI and LSI with a Si–Zr alloy, and studied its ablation characteristics. The results showed no significant reduction in linear ablation rates compared to C/C–ZrC composites. Kong et al. [14] created a Cf/SiC-ZrB_2 composite via the SI and LSI processes. They evaluated its ablation performance, finding a notable decrease in both mass and linear ablation rates due to the formation of a protective ZrO_2 layer on the surface. ZrB_2

[DOI: 10.22068/ijmse.3880]

is recognized as a highly promising ultra-high temperature ceramic (UHTC), with properties such as low density (6.085 g/cm³), a high melting point (~3000°C), an elastic modulus of ~440–460 GPa, and a hardness of ~20–25 GPa [15]. Boride ceramics exhibit greater thermal conductivity than carbide ceramics, vital for effective heat dissipation in regions with concentrated heat [16]. While most studies focus on the mechanical properties of C/C composites [17–19], only a few have addressed the ablation behavior of 3D needle-punched C/C-SiC composites [20–22]. Additionally, there remains a gap in research on the ablation behavior of C/C-SiC-ZrB_2 composites utilizing 3DW preforms.

Therefore, a newly fabricated three-dimensional orthogonal woven carbon fiber preform was selected in this work. The C/C-SiC-ZrB_2 composites were produced through a combination of I-CVI, SI, and LSI methods, making it one of the most recent and cost-effective approaches for manufacturing these composites. The porous C/C–ZrB_2 preforms were created via SI and then infiltrated with a Si alloy at 1650°C to form C/C–SiC–ZrB_2 composites. The SiC matrix was generated by the reaction between carbon and silicon during the LSI process, while the ZrB_2 matrix was introduced directly through slurry impregnation. The study also explored the microstructure and ablation performance of the C/C−SiC-ZrB_2 composites.

2. EXPERIMENTAL PROCEDURES

Figure 1 illustrates fabricating C/C-SiC-ZrB_2 composites using I-CVI, SI, and LSI methods. This study used a 3DW fabric made from T-300 (6K) carbon fiber, with a density of 0.48 g/cm³, as the preform. A carbon matrix was deposited into the 3DW preform via I-CVI at 1050°C using methane (CH4) as the precursor, creating a porous C/C structure. This was followed by a graphitization process at 2400°C with a heating rate of 5°C/min for one hour in a vacuum furnace with a 10^{-2} vacuum level. The temperature was then decreased to 1000°C by a -5°C/min and then furnace cooled to room temperature. The preform's density reached 0.83 g/cm³ with 48% open porosity. ZrB_2 powder with 99.99% purity and size distribution of 1-5 µm (Naiou Nano Technology Co., Ltd., Shanghai, China) comprised 40 wt% of the mixed slurry. An ethanol solution was used for six hours to prepare a high-solid-content ZrB_2 mixture via planetary ball milling with ZrO_2 balls. THC-800 phenolic resin with 95.0% purity (Shaanxi Taihang Fire Retardant Polymer Co., Ltd., Xi'an, China) was also added and acted as the carbon source of the matrix and also the binder for the ZrB_2.

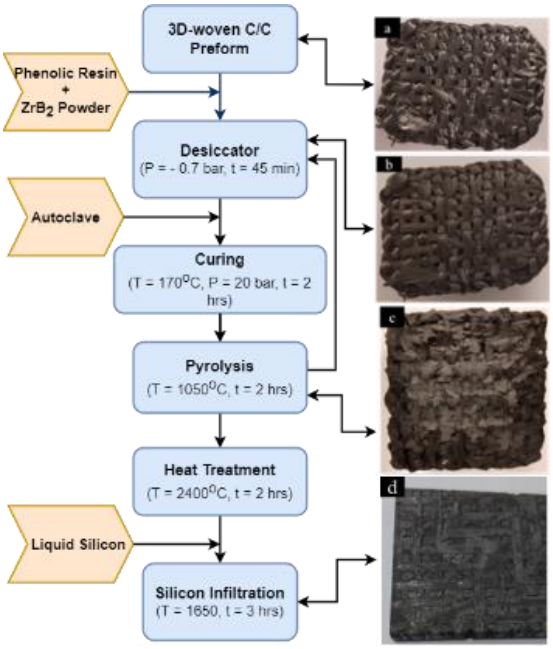

Fig. 1. Flow chart for the process of fabricating C/C-SiC-ZrB_2 composites by the combined process of I-CVI, SI and LSI, and Photographs of a) 3DW, b) 3DW + I-CVI, c) 3DW + I-CVI + SI and d) 3DW + I-CVI + SI + LSI preform

Figure 2 displays the morphology and XRD pattern of ZrB_2 particles. The slurry was then impregnated into the 3DW carbon fabric in a desiccator at a pressure of -0.7 bar for 45 minutes. Following this, the preform was treated in an autoclave under vacuum at 170°C for two hours, followed by pyrolysis and thermal treatment at 1050°C and 2400°C for two hours each. A C/C-ZrB_2 composite with a 1.54 g/cm³ density was obtained by repeating the impregnation-pyrolysis cycle three times. The 3DW preform was then placed in a graphite crucible with Si powder and heated to 1650°C for three hours in a vacuum environment at a constant pressure of 10^{-2} bar for the LSI process. Once the temperature surpassed the melting point of silicon (Tm= 1415°C), the liquid silicon became more fluid, allowing it to penetrate the micro-cracks formed during carbonization.

[DOI: 10.22068/ijmse.3880]

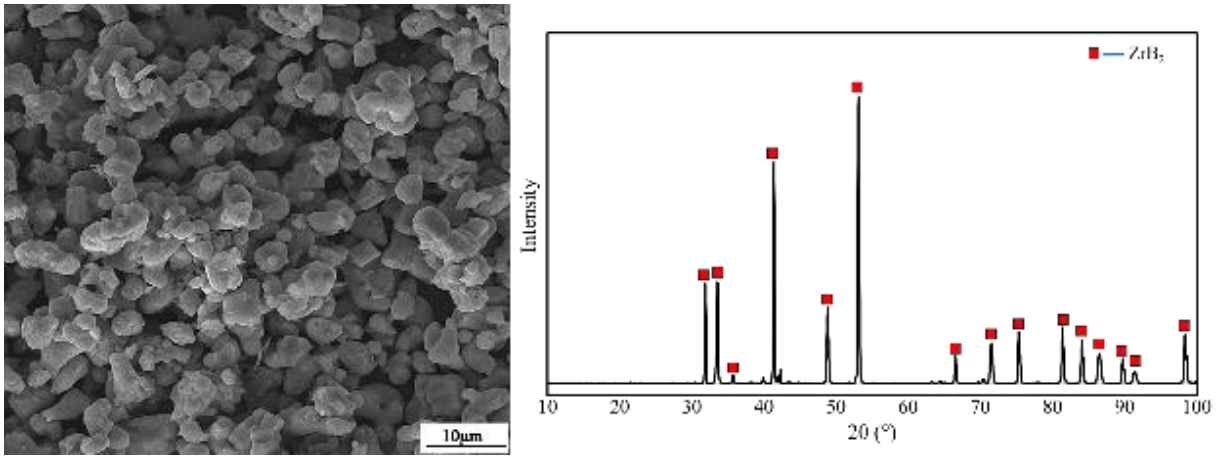

Fig. 2. The morphology and X-ray diffraction pattern of ZrB_2 powder

The molten Si infiltrated the preform through capillary action along the carbon fibers, where it reacted with the carbon to create the SiC matrix. The phase composition of the C/C-SiC-ZrB_2 composite was determined using an X-ray diffractometer (XRD; GNR, Italy) with CuKα1 radiation at room temperature. The density and open porosity of the specimens were measured using Archimedes' method, with values averaged from five tests. The ablation characteristics of the samples were evaluated with an oxyacetylene torch. The pressure and flow rate for C_2H_2 were set at 0.095 MPa and 0.31 L/s, while for O_2, they were 0.4 MPa and 0.42 L/s. The specimens were exposed to the flame for 120 seconds. The nozzle tip had an internal diameter of 2.0 mm, and the distance between the samples and the nozzle was set at 10 mm. Using an optical pyrometer, the surface temperature at the center of the samples reached 2500°C. The linear and mass ablation rates of the samples were calculated using Equations (1) and (2), respectively:

$$R_l = (d_0 - d_1)/t \quad (1)$$

$$R_m = (m_0 - m_1)/t \quad (2)$$

Where R_l is the linear ablation rate; d_0 and d_1 are the thickness values of samples in the center region before. After ablation, R_m is the mass ablation rate, m_0 and m_1 are the masses of the samples before and after ablation, respectively, and t is the ablation time. The microstructure and elemental distribution of the composites were examined using a field emission scanning electron microscope (FESEM) and an energy dispersive spectroscope (EDS) (MIRA3, TESCAN, Czech).

3. RESULTS AND DISCUSSION

3.1. Microstructure of as-Built C/C–ZrB_2–SiC Composite

The density and porosity of the C/C, C/C-SiC, and C/C-SiC-ZrB_2 composites are displayed in Table 1. When compared with C-C (1.81 g/cm^3), C-C-SiC (1.92 g/cm^3), 2D C_f/SiC-ZrB_2 (2.36 g/cm^3) [20], 2D C_f/SiC-ZrB_2 (2.1 g/cm^3) [28], 2D C/SiC-ZrB_2-ZrC (2.23 g/cm^3) [18] and 2D C/SiC- ZrB_2-TaC (2.35 g/cm^3) [29] composites, the C/C- SiC-ZrB_2 (2.38 g/cm^3) composite has a relatively higher density and lower porosity due to the high-solid content (ZrB_2 particles) of the added slurry and lower viscosity and flow resistance into the loose and porous 3DW preform. Additionally, the molten silicon reacts with the carbon fibers in the 3DW preform (point 1 in Fig 5c) at 1650°C, forming SiC.

Table 1. Open porosity and density in the C/C, C/C-SiC and C/C–SiC-ZrB_2 composites

Samples	Density (gr/cm^3)	Open Porosity (%)
C/C	1.71	22.7
C/C-SiC	1.92	10.5
C/C-SiC-ZrB_2	2.38	9.3
2D C_f/SiC-ZrB_2 [20]	2.36	10.7
2D C_f/SiC-ZrB_2 [28]	2.10	-
2D C/SiC-ZrB_2-ZrC [18]	2.23	10
2D C/SiC– ZrB_2–TaC [29]	2.35	11.5

[DOI: 10.22068/ijmse.3880]

This reaction enhances the density and reduces the porosity of the C/C–SiC-ZrB_2 composite by filling the pores within the porous 3DW C/C–ZrB_2 structure. The LSI process offers a cost-effective, rapid, and efficient technique for producing composites with high density and low porosity [20].

Figure 3 presents the microstructures and EDS analysis of porous C/C and C/C-ZrB_2 composites, which have not yet been introduced to the silicon infiltration. The gaps in the densely packed fiber bundle areas are filled with pyrolytic carbon layers, approximately 2.5 µm thick (Fig 3a). As shown in Fig. 3b, ZrB_2 powders are distributed almost uniformly, coating the carbon fibers. The porous 3DW C/C–ZrB_2 composite contains varying-sized voids, providing infiltration paths for molten Si alloy during the LSI process. The even distribution and stability of ZrB_2 particles help form a nearly uniform microstructure after the LSI process, which enhances the ablation resistance of the C/C-SiC-ZrB_2 composite. EDS analysis was conducted on different areas of the C/C and C/C-ZrB_2 composites cross-sections, as shown in Fig. 3c, d, and e.

Fig. 4 shows the polished cross-sectional microstructures of the C/C–SiC-ZrB_2 composite following the I-CVI, SI, and LSI processes. The scattered voids within the fiber bundles are filled with carbon, SiC, and ZrB_2. The voids between the pyrolytic carbon layers and ZrB_2 particles (as shown in Fig. 3b) are occupied mainly by the newly formed SiC ceramic. In Fig. 4a, the ZrB_2 particles exhibit a nearly uniform distribution across the matrix. Additionally, micro-cracks observed in the C/C-SiC–ZrB_2 composite likely result from the infiltration of the Si alloy into the channels of the 3DW preform. The SiC matrix formation, driven by the reaction between molten Si, pyrolytic carbon, and carbon fibers, is highly exothermic. The difference in thermal expansion coefficients between SiC (4×10^{-6} K^{-1}) and carbon ($2\text{-}4 \times 10^{-6}$ K^{-1}) is the primary cause of these micro-cracks, as seen in Fig. 4b [30, 31].

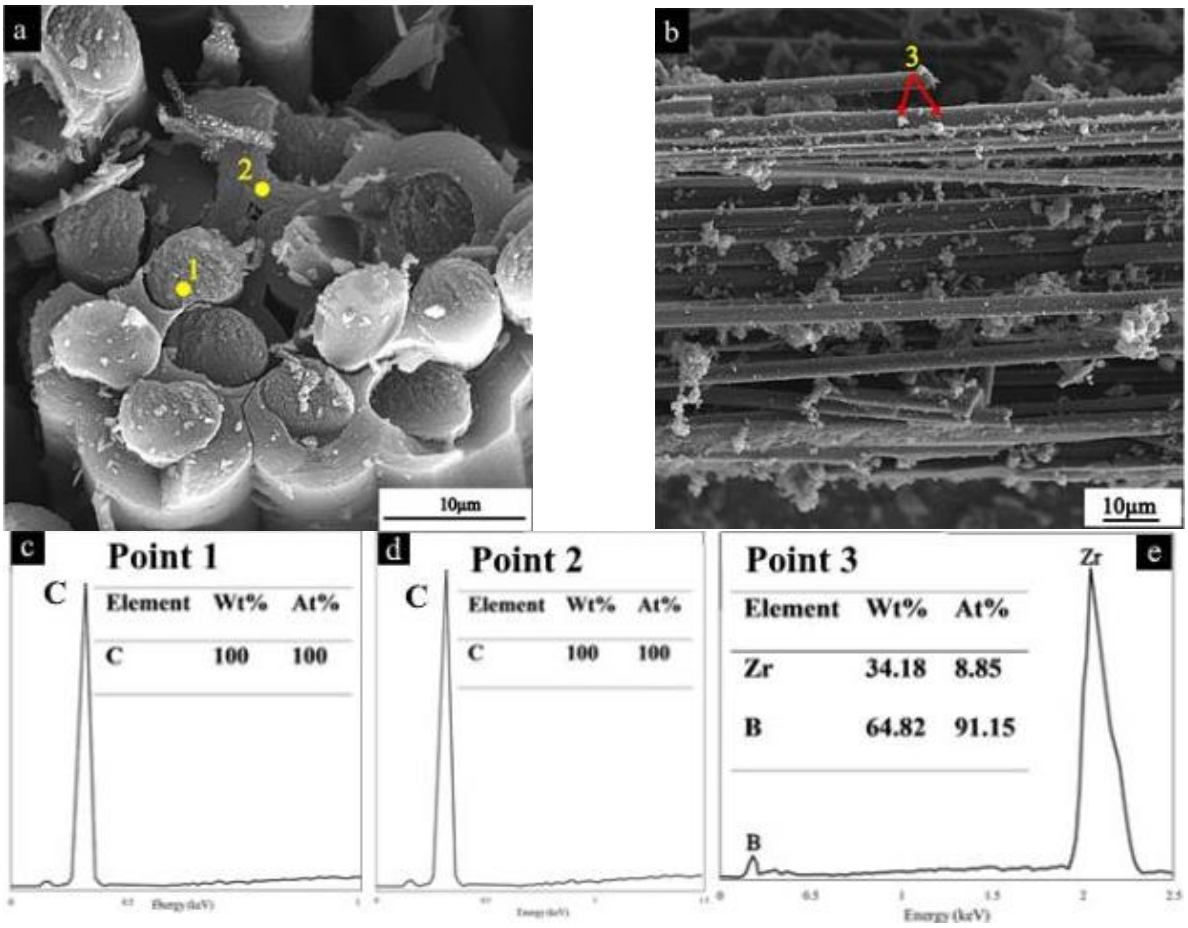

Fig. 3. a and b) SEM images of the microstructure of C/C and C/C-ZrB_2 composites (before the LSI process) and c, d and e) EDS analyses of the indicated points

[DOI: 10.22068/ijmse.3880]

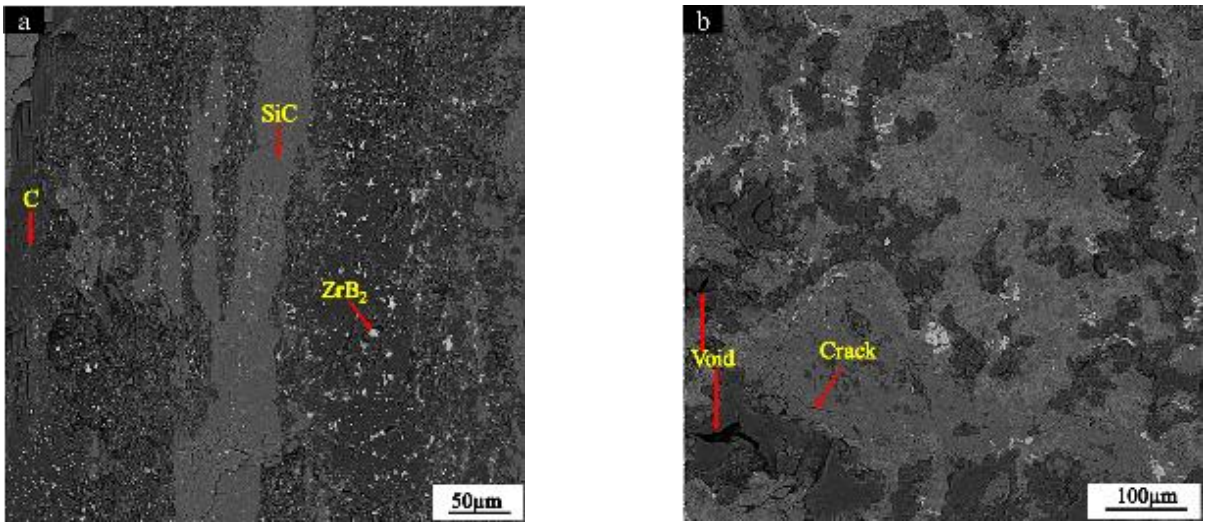

Fig. 4. Cross-sectional microstructures of the C/C–SiC-ZrB_2 composite: a) micro-cracks and b) scattered voids

Fig. 5a, b, c, and d show the intricate microstructure of the C/C–SiC–ZrB_2 composite. The four contrasted zones that fill the inter-bundles are as follows: dark gray, white, medium gray, and light gray, which represent C, ZrB_2, SiC, and Si, respectively. With a few tiny voids, the resulting matrix is dense. The C/C–SiC–ZrB_2 composite was subjected to the EDS examination at various locations (Fig. 5e–h). At point 1, adjacent to the carbon source and fiber bundle, only SiC is present. Further from this point, silicon starts to appear in the matrix, with higher concentrations nearer the center of the matrix (as shown in Fig. 5f, point 2). Although the infiltrated silicon is expected to react fully with the carbon source and fibers, some residual silicon was found between the SiC matrices. Point 3 identifies the carbon source resulting from the phenolic resin pyrolysis. Point 4 highlights the presence of ZrB_2 particles located in the center of the C/C–SiC–ZrB_2 composite (Fig. 5e). Fig. 6 displays an SEM image and EDS mapping of the C/C–SiC–ZrB_2 composite. It comprises an interpenetrating microstructure consisting of four phases: C, Si, SiC, and ZrB_2. Based on the EDS maps, the C/C–SiC–ZrB_2 composite surface contains Zr, B, Si, and C.

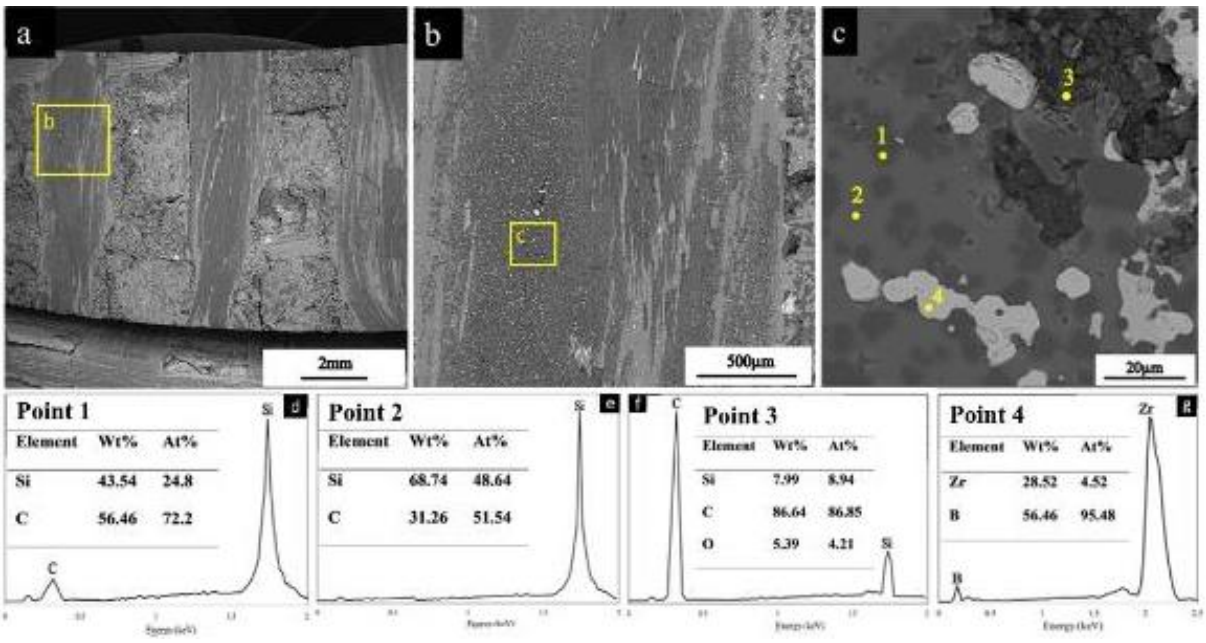

Fig. 5. a-c) Back-scattered electron images of the cross sections of C/C–SiC–ZrB_2 composite, and e-h) EDS analyses of different spots

[DOI: 10.22068/ijmse.3880]

These data, combined with XRD findings (Fig. 7), conclude that the composite surface regions include four main phases: C, Si, SiC, and ZrB_2. Additionally, the relatively uniform distribution of ZrB_2 particles in the microstructure is evident from the SEM image. This uniform distribution of ZrB_2 particles creates a completely uniform protective ZrO_2 oxide layer on the C/C–SiC–ZrB_2 composite surface after the oxyacetylene test, which ultimately prevents the penetration of oxygen into underlying layers and the oxidation of the C/C–SiC–ZrB_2 composite.

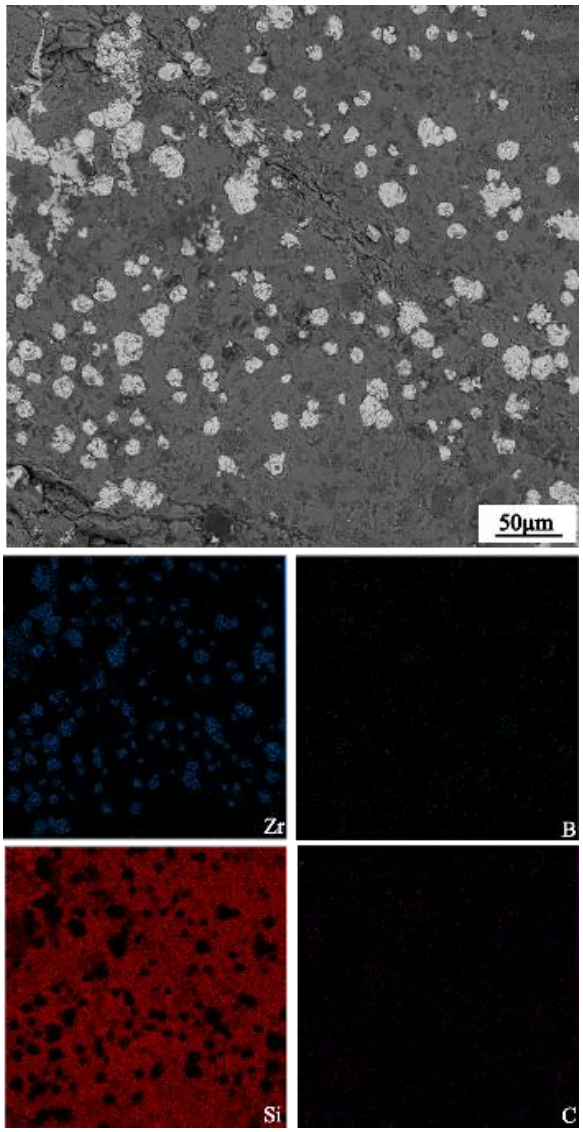

Fig. 6. SEM image and EDS mapping or a representative C/C–SiC–ZrB_2 composite area

Fig. 7 displays the crystalline phases present in the C/C-SiC-ZrB_2 composite after fabrication. The primary phases identified in the composite are ZrB_2, SiC, and carbon. XRD also reveals a minor presence of $ZrSi_2$, probably due to a reaction between remnant molten silicon and the ZrB_2. While the LSI process is an efficient, cost-effective method for producing high-density C/C-SiC-ZrB_2 composites, the presence of residual silicon reduces the composite's ablation resistance. Analysis from XRD and EDS (shown in Figs. 5 and 6) confirms that most of the infiltrated silicon has reacted with the carbon to form the SiC matrix.

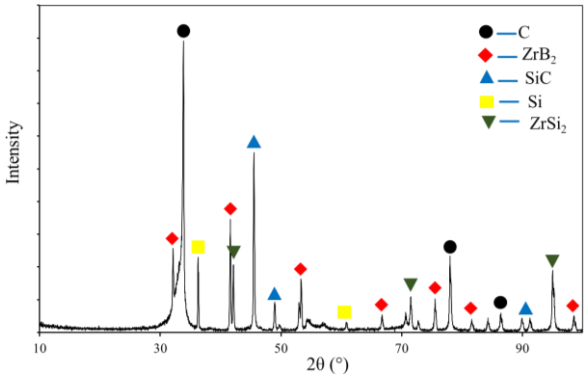

Fig. 7. X-ray diffraction patterns of different C/C–SiC–ZrB_2 composite

3.2. Formation Mechanism of the C/C–SiC–ZrB_2 Composite

Fig. 8 illustrates the structural evolution of the C/C–SiC–ZrB_2 composite through the innovative combined process of I-CVI, SI, and LSI.

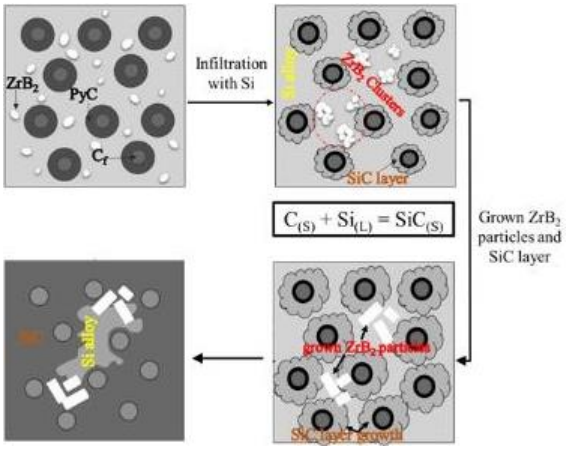

Fig. 8. Depiction of the changes in microstructure and the formation process of C/C–SiC–ZrB_2 composites during the LSI process

Initially, when the molten silicon alloy is introduced into the porous C/C–ZrB_2 preform, carbon atoms dissolve and react with silicon to

[DOI: 10.22068/ijmse.3880]

form a continuous and substantial SiC layer. Subsequently, ZrB_2 particles, which are not fixed by carbon resin, are rearranged due to the surface tension of the molten silicon, resulting in the formation of large, integrated clusters. Research has shown that the presence of the liquid alloy among ZrB_2 particles of varying sizes can enhance mass transfer and facilitate the migration of grain boundaries. Smaller particles dissolve within the ZrB_2 clusters, penetrate the melt, and crystallize onto larger particles, creating irregular spaces between the growing ZrB_2 particles. In summary, while the ZrB_2 particles' penetration does not significantly impact the C and Si reaction process, the melt promotes the growth of ZrB_2 particles, which can affect the uniformity of ZrB_2 distribution within the C/C–SiC–ZrB_2 composite.

3.3. Ablation Resistance Behavior of C/C-SiC-ZrB_2 Composite

Fig. 9 displays macroscopic photographs of the C/C-SiC-ZrB_2 composite before and after the ablation test at a temperature of 2500°C for 120 seconds. The LSI-processed sample, measuring 40 mm × 40 mm and shown in Fig. 9a, was subjected to an oxyacetylene torch test for 120 seconds. Post-ablation, the coating surface was categorized into three distinct areas: the outer edge ©, the transition zone near the center (B), and the central area (A) (Fig. 9b). The ablated surface of the C/C-SiC–ZrB_2 composites shows a white, loose layer. As illustrated in Fig. 9, this white layer becomes more prominent with extended ablation times, reaching up to 120 seconds. This layer likely consists of oxidation products from the composite's primary components. The most intense ablation is observed at the flame's center. Given that the oxyacetylene torch flame reaches 2500°C, the ZrB_2-SiC in the composite reacts with oxygen, rapidly forming ZrO_2 and SiO_2 phases on the surface. To determine the linear and mass ablation rates, the dimensions and mass of the samples were measured before and after the ablation test. Fig. 10 (a and b) presents the linear and mass ablation rates for the C/C-SiC–ZrB_2 composite. For comparison, the ablation rates of C/C, C/C-SiC, and C/C-SiC-ZrB_2 are also displayed in Fig. 10 (a and b). Of these composites, C/C-SiC-ZrB_2 demonstrates the highest ablation resistance in oxyacetylene torch tests. Fig. 10 provides a comparison of the linear and mass ablation rates for 2D C/C-SiC-ZrB_2 [20], 3D C/C-SiC-ZrC [17], 2D C/SiC-ZrB_2-ZrC [18], and C/C-SiC-ZrB_2. Among these materials, C/C-SiC-ZrB_2 exhibits the highest linear ablation resistance when exposed to oxyacetylene torch conditions.

According to Fig. 10, the linear and mass ablation rates of the C/C-SiC-ZrB_2 composite are 1.4 μm/s and 2.2 mg/s at 120 seconds, respectively. This indicates that the weight of the C/C-SiC-ZrB_2 composite has decreased after the ablation due to the generation and evaporation of oxide products. This is due to the C/C-SiC-ZrB_2 composite withstanding high-temperature exposure for 120 seconds during the ablation test. Under these conditions, some oxide products such as CO, CO_2, SiO, SiO_2, and B_2O_3 evaporate and exit from the surface. Among these composites, C/C-SiC-ZrB_2 exhibits the highest ablation resistance in the oxyacetylene torch environment, attributed to the high ZrB_2 particle loading achieved through slurry impregnation and as can be seen, the present C/C-SiC-ZrB_2 composite with a 3DW preform has a higher resistance to ablation compared to the composites investigated in [17, 18, 20] due to the higher density of carbon fibers in all dimensions, increase in the amount of ZrB_2 particles trapped in the preform, and reducing the overall porosity. Additionally, the XRD pattern (Fig. 12), along with the microstructural and EDS analysis (Fig. 11a) of the ablated sample's surface, reveals that the white layer is composed of ZrO_2. This ZrO_2 layer acts as a barrier, restricting further oxygen diffusion into the composite and thereby reducing additional ablation.

Fig. 11 (a−f) shows the BSE images and EDS analysis of the microstructures from the center, transition, and edge regions of the C/C-SiC-ZrB_2 composite after 120 seconds of ablation. At the center of the sample, where temperatures reach approximately 2500°C, the rapid oxidation of ZrB_2 and SiC forms a dense layer of ZrO_2 and SiO_2. This oxidation causes a significant loss of SiO_2 and B_2O_3, which contributes to an increased mass ablation rate and the formation of voids. The EDS analysis confirms that the white particles are ZrO_2 (Fig. 11b). Fig. 11c illustrates the microtopography of the transition area (B), showing a surface covered with rough, porous white and gray glass phases. According to Fig. 11d, EDS analysis of area B reveals that the layer consists of a mixture of SiO_2 and ZrO_2, which helps prevent further ablation.

[DOI: 10.22068/ijmse.3880]

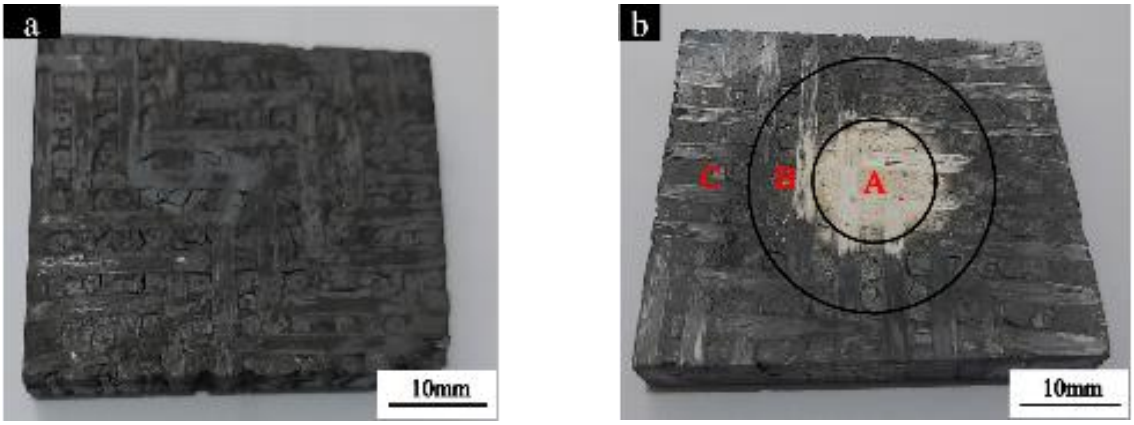

Fig. 9. Macroscopic images of the C/C-SiC-ZrB_2 composite a) before and b) after the oxyacetylene torch test

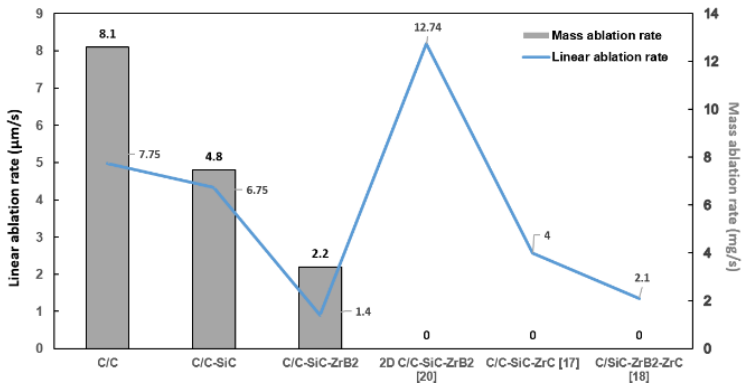

Fig. 10. Mass and linear ablation rates of variable composites

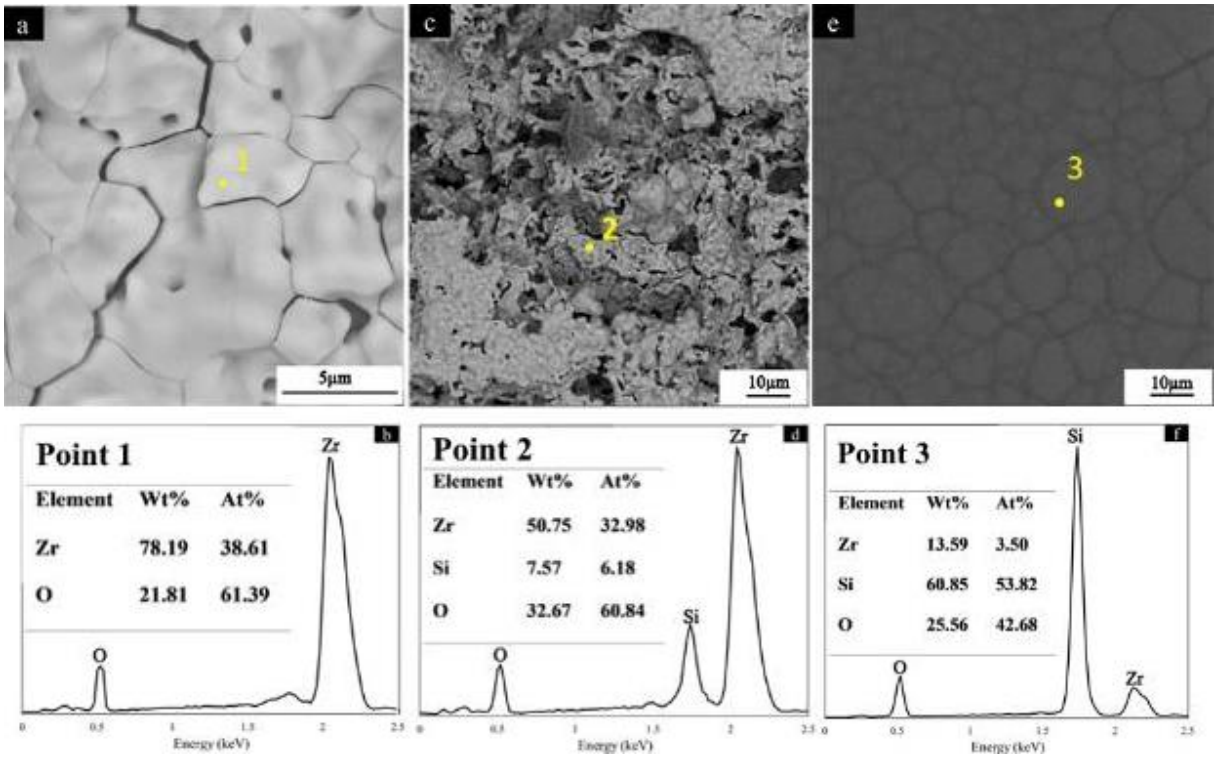

Fig. 11. Back-scattered electron images and EDS analyses of the C/C-SiC-ZrB_2 composite ablated surface in oxyacetylene flame: a) center, b) transition and c) border regions

[DOI: 10.22068/ijmse.3880]

In the transition oxidation region, where temperatures are lower than at the center, only a small amount of ZrO_2 forms, while most of the silicon oxides and evaporated B_2O_3 create numerous voids. The edge oxidation region is covered by a gray coating (Fig. 11e). The EDS results (Fig. 11f) indicate that the ablation products are primarily Si−Zr−O phases, with silicon as the dominant element. Few ZrB_2 particles are oxidized in this region due to the lower temperature compared to the transition zone. The matrix morphology in Figure 11e is representative of a chemical product, and the composition of the point 3 matches with $ZrSiO_4$ which is brought in the references. Sun et al. [32] demonstrated that $ZrSiO_4$ phase forms after the ablation test of a C/C-SiC-ZrB_2 composite produced by the same method used in the currect study. The Zr−Si−O phase has a higher melting point than SiO_2 and resists being blown away by gas flow, thus protecting the underlying fibers from oxidation.

Fig. 12 shows the crystalline phases present in the sample after the oxyacetylene torch test. The ablated surface of the C/C–SiC–ZrB_2 composites (Fig. 11a) features a white layer. The XRD pattern of this surface reveals that this white molten layer is composed solely of ZrO_2, formed from the oxidation of ZrB_2 ceramics. ZrO_2 remains stable at temperatures up to 2500°C due to its high melting point (2715°C), despite other potential reaction products. In contrast, SiO_2 rapidly evaporates at temperatures approaching 2500°C and is carried away by the fast-moving oxyacetylene torch in the central ablation zone. Similarly, B_2O_3, which has a low melting point of 450°C and a high vapor pressure that leads to its quick vaporization above 1100°C, also evaporates swiftly. The instability of SiC and B_2O_3 oxidation products at the flame tip explains the lack of SiO_2 and B_2O_3 peaks in the XRD pattern [23].

Fig. 13 presents the cross-sectional image of the C/C-SiC-ZrB_2 composite after undergoing the ablation test. The thickness of the surface oxide layer, primarily composed of ZrO_2, as approved by the map scanning presented in Fig. 14, measures 330 μm. During the oxyacetylene flame test, the surface layer of the composite is damaged and subsequently transformed into a protective oxide phase of ZrO_2. The oxide layer near the surface, consisting of ZrO_2, and the subsequent SiO_2 layer have a combined thickness of 42 μm. The lower layers of the composite, being in contact with the surface layer and exposed to lower temperatures, undergo a transformation of the continuous SiC phase into a protective SiO_2 oxide layer. This SiO_2 layer serves to inhibit oxygen penetration into the deeper layers of the composite.

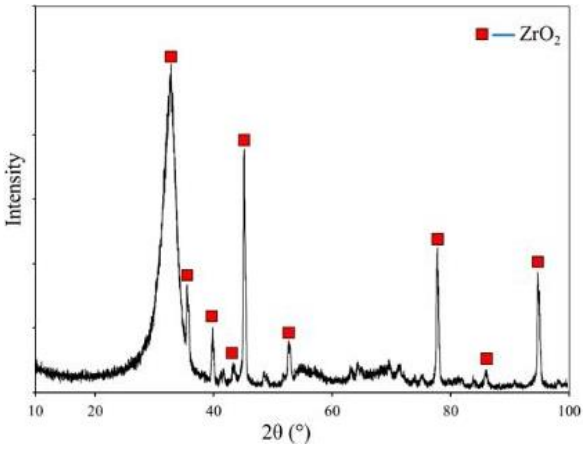

Fig. 12. X-ray diffraction pattern of C/C-SiC-ZrB_2 composites after being exposed to the oxyacetylene torch

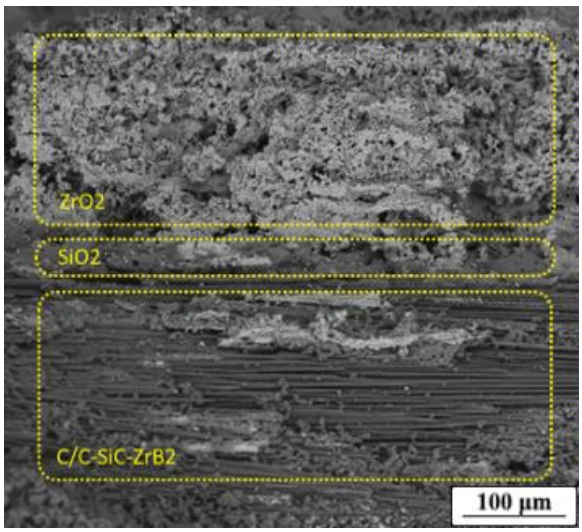

Fig. 13. Cross section of C/C-SiC-ZrB_2 composite after being exposed to the oxyacetylene torch

3.4. Ablation Mechanism

The reactions below might occur in the central region during the oxyacetylene torch ablation test [24, 25].

$$2C\ (s) + O_2\ (g) \rightarrow 2CO\ (g) \quad (1)$$

$$C\ (s) + O_2\ (g) \rightarrow CO_2\ (g) \quad (2)$$

$$2ZrB_2\ (s) + 5O_2\ (g) \rightarrow 2ZrO_2\ (s) + 2B_2O_3\ (g) \quad (3)$$

$$SiC\ (s) + 2O_2\ (g) \rightarrow SiO_2\ (l) + CO_2\ (g) \quad (4)$$

$$2SiC\ (s) + 3O_2\ (g) \rightarrow 2SiO_2\ (l) + 2CO\ (g) \quad (5)$$

[DOI: 10.22068/ijmse.3880]

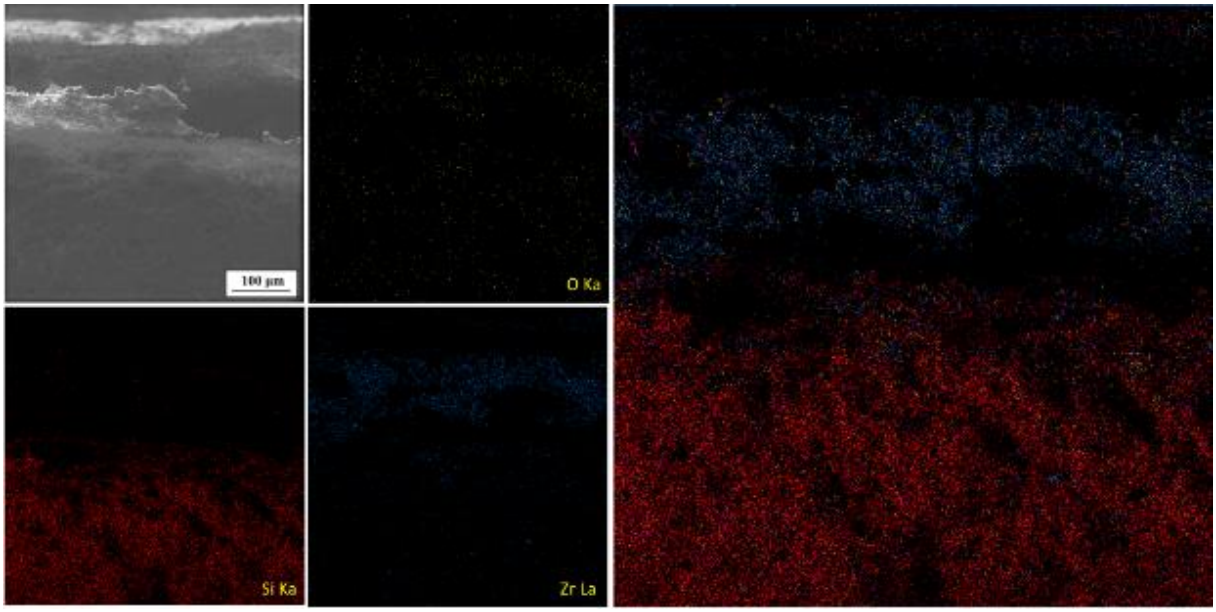

Fig. 14. Elemental map of the cross section of C/C-SiC-ZrB_2 composite after the oxyacetylene torch test

SiO_2 (l) → SiO_2 (g) (6)

SiO_2 (l) + CO (g) → SiO (g) + CO_2 (g) (7)

Si (g) + SiO_2 (l) → 2SiO (g) (8)

Fig. 15 illustrates the ablation process of the C/C-ZrB_2-SiC composite. At the start of ablation, the surface temperature of the composite rises quickly, and oxidative gases interact with the carbon fibers, carbon matrix, SiC, and ZrB_2 (Eqs. 1−8). The initial contact with the oxyacetylene torch flame leads to rapid oxidation of the carbon fibers (Eqs. 1 and 2). As the flame temperature increases, SiC and ZrB_2 react with oxygen, forming ZrO_2 and SiO_2 on the surface through reactions 3-5 at temperatures of 1100°C and 1500°C, respectively. These oxide phases help shield the carbon structure from further oxidation.

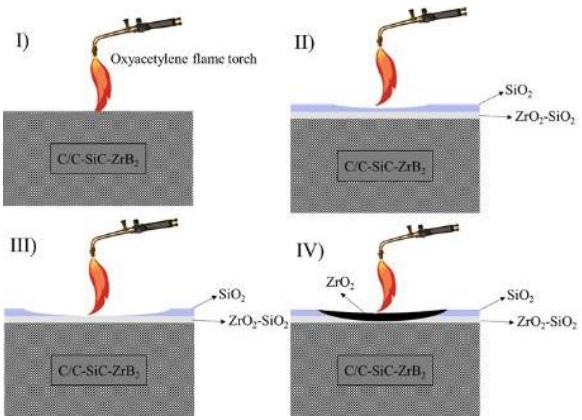

Fig. 15. Surface ablation phenomena of 3DW C/C-SiC-ZrB_2 composite

Once the temperature exceeds 1415°C, Si and SiO_2 start to melt and evaporate due to the high-pressure combustion gases (Eqs. 6-8). Furthermore, ZrB_2 particles near the surface produce a ZrO_2 layer with a high melting point (2850°C), resulting in a thick, viscous ZrO_2-SiO_2 layer. This robust ZrO_2 layer, formed and densified at high temperatures, effectively blocks additional oxygen from penetrating the composite and thus prevents further ablation. At temperatures around 2500°C, intense oxidation from reaction 4 may damage the SiC matrix [26, 27]. However, the dense ZrO_2 layer helps alleviate this oxidation, thereby preserving the SiC matrix.

4. CONCLUSIONS

The innovative 3D orthogonal woven C/C-SiC-ZrB_2 composite was produced using a combined technique of I-CVI, SI, and LSI, involving Si alloy infiltration and chemical reactions at 1650°C. The composite's mass and linear ablation rates were evaluated using an oxyacetylene torch test. Compared to the bare C/C and C/C-SiC composites, the C/C-SiC-ZrB_2 composite demonstrated superior ablation resistance. Specifically, the mass and linear ablation rates of the C/C-SiC-ZrB_2 composite were 1.4 µm/s and 2.2 mg/s, respectively, at 120 seconds. At high temperatures, residual Si in the composite melted to form a protective SiO_2 layer on the surface. However, the SiC matrix was susceptible to oxidation and evaporation from

[DOI: 10.22068/ijmse.3880]

the high-speed torch flame, failing to fully shield the carbon fibers. The incorporation of ZrB_2 into the C/C-SiC composite, achieved through the LSI process, markedly reduced both the linear and mass ablation rates by creating a dense ZrO_2 layer with low open porosity. This high-temperature-sintered ZrO_2 layer effectively blocked further oxygen penetration into the composite and mitigated additional ablation. Adequate ZrB_2 content enhanced the composite's ablation and oxidation resistance by continuously generating ZrO_2 to safeguard the surface.

REFERENCES

[1] Su-fang, T., Jing-yi, D., Shi-jun, W., Wen-chuan, L., "Comparison of thermal and ablation behaviors of C/SiC composites and C/ZrB_2−SiC composites". Corr. Sci., 2009, 51, 54−61.

[2] He-jun, L., Xi-yuan, Y., Yu-lei, Z., Ke-zhi, L., Ling-jun, G., Lei, L., "Effect of heat flux on ablation behaviour and mechanism of C/C−ZrB_2−SiC composite under oxyacetylene torch flame". Corr. Sci., 2013, 74, 265−270.

[3] Li-ping, R., Fei, R., Ke, P., Huan, Y., Mao-zhong, Y., "Preparation and properties of C/C−ZrB_2−SiC composites by high-solid-loading slurry impregnation and polymer infiltration and pyrolysis (PIP)". Trans. Nonferrous Met. Soc. China, 2019, 29, 2141−2150.

[4] Ping, T., Liyong, T., G.P., S., Takashi, I., "Behavior of 3D orthogonal woven CFRP composites. Part I. Experimental investigation". Compos. Part A, 2000, 31, 259–271.

[5] Xue, H., Zhang, L., Cheng, L., "The effect of Z-yarn density on the in-plane shear property of three-dimensional stitched carbon fiber reinforced silicon carbide composites". Comp. Sci. Technol., 2015, 106, 120–126.

[6] Mei, H., Liang, C., Zhang, D., Chen, C., Cheng, L., "Controlled deposition of density defects for understanding mechanical reduction on 2D C/SiC composites". Comp. Part B, 2019, 161, 241–251.

[7] Tang, S.F., Deng, J.Y., Wang, S.J., Liu, W.C., "Fabrication and characterization of an ultra-high temperature carbon fiber-reinforced ZrB_2–SiC matrix composite". J. Am. Ceram. Soc., 2007, 90, 3320–3322.

[8] Li, Q.G., Dong, S.M., Wang, Z., He, P., Zhou, H.J., Yang, J.S., Wu, B., Hu, J.B., "Fabrication and properties of 3D Cf/SiC–ZrC composites, using ZrC precursor and polycarbosilane". J. Am. Ceram. Soc., 2012, 95, 1216–1219.

[9] Tulbez, S., Esen, Z., Dericioglu, A.F., "Effect of CNT impregnation on the mechanical and thermal properties of C/C-SiC composites". Adv. Comp. Hybrid Mater., 2020, 3, 177–186.

[10] Zhou, H.J., Ni, D.W., He, P., Yang, J.S., Hu, J.B., Dong, S.M., "Ablation behavior of C/C-ZrC and C/SiC-ZrC composites fabricated by a joint process of slurry impregnation and chemical vapor infiltration". Ceram. Int., 2018, 44, 4777–4782.

[11] Yiguang, W., Xiaojuan, Z., Litong, Z., Laifei, C., "C/C–SiC–ZrC composites fabricated by reactive melt infiltration with Si0.87Zr0.13 alloy". Ceram. Int., 2012, 38, 4337–4343.

[12] Mei, H., Cheng, L., "Comparison of the mechanical hysteresis of carbon/ceramic-matrix composites with different fiber preforms". Carbon, 2009, 47, 1034–1042.

[13] Seyoung, K., In Sub, H., Young-Hoon, S., Do Kyung, K., "Mechanical properties of C–SiC composite materials fabricated by the Si–Cr alloy melt-infiltration method". J. Comp. Mater., 2015, 49, 3057–3066.

[14] Jung Hoon, K., Seung Yong, L., Young Il, S., Do Kyung, K., "Synergistic reinforcement effects of ZrB_2 on the ultra-high temperature stability of Cf/SiC composite fabricated by liquid silicon infiltration". J. Eur. Ceram. Soc., 2023, 43, 3062–3069.

[15] Mrumun David, T., Anejo, I., "Effects of surface modification (surface treatment) on friction and surface abrasion of ceramic composites". Adv. Ceram. Mater., 2023, 91–114.

[16] Jin, X., Fan, X., Lu, C., Wang, T., "Advances in oxidation and ablation resistance of high and ultrahigh temperature ceramics modified or coated carbon/carbon composites". J. Eur. Ceram. Soc., 2018, 38, 1–28.

[17] Wang, Y.G., Zhu, X.J., Zhang, L.T., "C/C-SiC-ZrC composites fabricated by reactive

[DOI: 10.22068/ijmse.3880]

melt infiltration with Si0.87Zr0.13 alloy". Ceram. Int., 2012, 38, 4337–4343.
[18] Huilong, P., Shangwu, F., Yiguang, W., "C/SiC–ZrB_2–ZrC composites fabricated by reactive melt infiltration with $ZrSi_2$ alloy". Ceram. Int., 2012, 38, 6541–6548.
[19] Du, XB., Li, DS., Wei, QH., Jiang, L., "High temperature bending properties and failure mechanism of 3D needled C/SiC composites up to 2000°C". J. Eur. Ceram. Soc., 2022, 42, 3036–3043.
[20] Fan, X., Dang, X., Ma, Y., Yin, X., Zhang, L., Cheng, L., "Microstructure, mechanical and ablation behaviour of C/SiC–Si with different preforms". Ceram. Int., 2019, 45, 23104–23110.
[21] Li, W., Xiang, Y., Wang, S., Ma, Y., Chen, Z., "Ablation behavior of three-dimensional braided C/SiC composites by oxyacetylene torch under different environments". Ceram. Int., 2013, 39, 463–468.
[22] Lei, L., He-jun, L., Kui, H., Xiao-hong, S., Ke-zhi, L., Chang, N., "Effect of SiC location on the ablation of C/C-SiC composites in two heat fluxes". J. Mater. Sci. Technol., 2015, 31, 345–354.
[23] Yue, L., Qian-gang, F., Bei-bei, W., Tian-yu, L., Jia, S., "The ablation behavior and mechanical property of C/C−SiC−ZrB_2 composites fabricated by reactive melt infiltration". Ceram. Int., 2017, 43, 6138–6147.
[24] Han, J.C., Hu, P., Zhang, X.H., Meng, S.H., Han, W.B., "Oxidation-resistant ZrB_2–SiC composites at 2200°C". Comp. Sci. Technol., 2008, 68, 799–806.
[25] Ping, H., Wang, G.L., Wang, Z., "Oxidation mechanism and resistance of ZrB_2–SiC composites". Corr. Sci., 2009, 51, 2724–2732.
[26] Lee, S.J., Kim, D.K., "Effect of TaB_2 addition on the oxidation behaviors of ZrB_2-SiC based ultra-high temperature ceramics". Korean J. Mater. Res., 2010, 20, 217–222.
[27] Balat-Pichelin, M., Charpentier, L., Panerai, F., Chazot, O., Helber, B., Nickel, K., "Passive/active oxidation transition for CMC structural materials designed for the IXV vehicle re-entry phase". J. Eur. Ceram. Soc., 2015, 35, 487–502.
[28] Wang, Y.G., Liu, W., Cheng, L.F., Zhang, L.T., "Preparation and properties of 2D C/ZrB_2–SiC ultra-high temperature ceramic composites". J. Appl. Ceram. Technol., 2009, 524, 129–133.
[29] Li, L.L., Wang, Y.G., Cheng, L.F., Zhang L.T., "Preparation and properties of 2D C/SiC–ZrB_2–TaC composites". Ceram. Int., 2011, 34, 891–896.
[30] Baxter, R.I., Rawlings, R.D., Iwashita, N., Sawada, Y., "Effect of chemical vapor infiltration on erosion and thermal properties of porous carbon/carbon composite thermal insulation". Carbon, 2000, 38, 441–449.
[31] Fahrenholtz, W.G., Hilmas, G.E., Talmy, I.G., Zaykoski, J.A., "Refractory biborides of zirconium and hafnium". J. Am. Ceram. Soc., 2007, 90, 1347–1364.
[32] Sun, Q., Zhang, H., Huang, C., Zhang, W., "Fabrication of C/C–SiC–ZrB_2 ultra-high temperature composites through liquid–solid chemical reaction". Crystals, 2021, 11, 1352.

[DOI: 10.22068/ijmse.3880]